CrossMark

ORIGINAL PAPER

Effect of graphene oxide on thermal stability of aerogel bio-nanocomposite from cellulose-based waste biomass

Sinyee Gan · Sarani Zakaria · Chin Hua Chia · Hatika Kaco

Abstract   By combining the waste of oil palm empty fruit bunch (EFB) and graphene oxide (GO), a GO/cellulose aerogel bio-nanocomposite was produced via a simple mixing method. The thermal properties of this nanocomposite were examined using thermogravimetric analysis (TGA), and the GO/cellulose aerogel bio-nanocomposite exhibited good thermal stability indicated by a delay in the degradation of the nanocomposite even at low GO incorporation. Experimental and modeled TGA curves were compared. The morphology of the GO/cellulose aerogel composite was observed under field emission scanning electron microscope. In GO/cellulose aerogel composite with 4 wt% GO, the pore volume and porosity decreased by more than 50% compared to aerogel without GO, and the density of the 4 wt% GO/cellulose aerogel composite showed a onefold increase compared with the pure cellulose aerogel. The degree of swelling and equilibrium-swelling ratio of regenerated GO/cellulose hydrogel and aerogel decreased with the higher GO concentration. The phase transition from EFB to regenerated GO/cellulose aerogel composite was evaluated using X-ray diffraction. This study has provided a simple pathway to produce environmentally friendly biocomposite materials.

S. Gan (✉) · S. Zakaria (✉) · C. H. Chia · H. Kaco
Bioresources and Biorefinery Laboratory, Faculty of
Science and Technology, Universiti Kebangsaan
Malaysia, 43600 Bangi, Selangor, Malaysia
e-mail: gansinyee@hotmail.com

S. Zakaria
e-mail: szakaria@ukm.edu.my

🍃 Springer

Graphical abstract
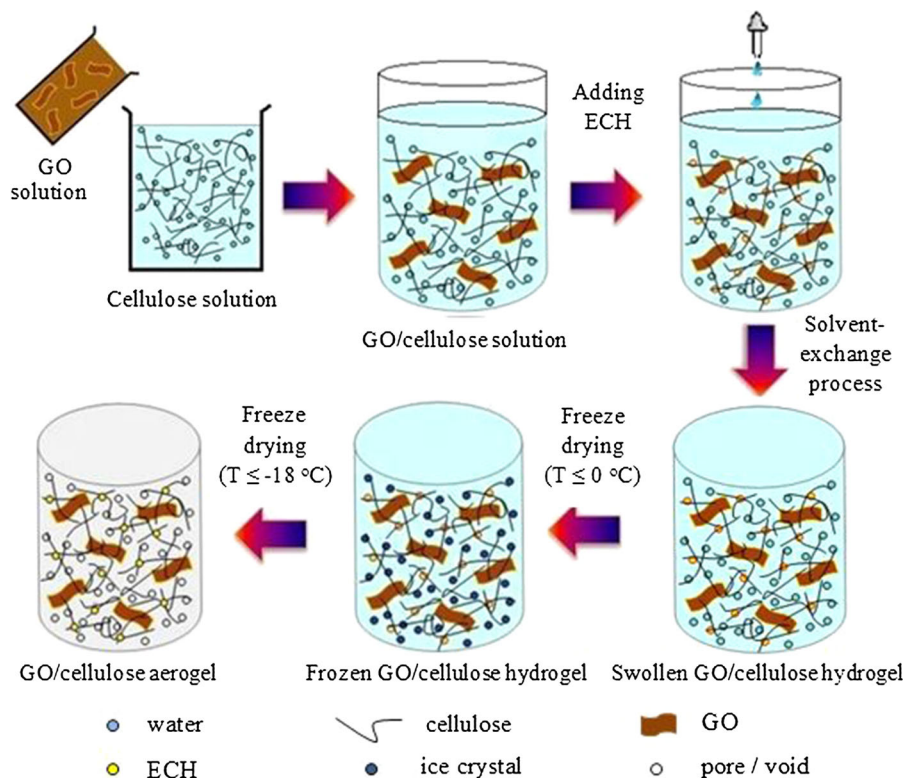
Keywords Agricultural waste · Bio-based material · Hydrogel · Nanomaterial · Regenerated cellulose

Introduction

The unsustainable consumption of petroleum-based products, the growth in environmental awareness, and new environmental regulations have created a need for environmentally-friendly biomaterials (Tozluoglu et al. 2018). Lignocellulosic biomass is a cheap, abundant, and renewable feedstock, applicable for biochemical purposes and biofuel production (Azahari et al. 2017). The total weight of oil palm byproducts consist mainly of trunk, shell, palm press fiber, frond, and empty fruit bunch (EFB). Production may exceed 90 million metric tonnes, in which the majority of the byproducts are EFB. Moreover, every ton of fresh fruit bunches could produce around 0.22 ton of EFB (Ahmadzadeh and Zakaria 2007). Therefore, new approaches should be developed in order to utilize the

EFB as value-added products, as highlighted in Malaysian National Biomass Strategy 2020 (Agensi Inovasi Malaysia 2016). There have been several developments of value-added EFB materials. Mohd Nor et al. (2015) successfully produced a carbon-monolith electrodes for supercapacitor from EFB with the aid of gamma (γ) radiation. Several pretreatments such as acid hydrolysis and thermal hydrolysis have been given to EFB to make it soluble. Dissolved EFB cellulose can be used to regenerate cellulose materials such as cellulose hydrogel and aerogel as reported by Ng et al. (2015). The production of bio products (such as films and aerogels) from renewable resources (such as waste biomass, starch, and lignin) has attracted a great deal of attention from researchers (Poyraz et al. 2017a, b; Tozluoğlu et al. 2017). Aerogels in partic- ular have extensive applications in thermal insulating materials, acoustic insulating materials, reinforcing materials, kinetic energy absorbers, scaffolds as they are biodegradable and environmentally friendly, char- acterized by low heat conductivity, large inner surface area, and have ultra-low density (Zhang et al.

2012a, 2017b). There has also been a recent surge of interest in bionanocomposites due to their low density, excellent mechanical properties, biodegradability, renewabaility, and biocompatibility. For example, Sarwar et al. (2018) prepared the PVA/nanocellulose/Ag nanocomposite films for antimicrobial food packaging. Besides that, the bionanocomposites can be prepared from different pulp sources, such as when Tozluoğlu et al. (2018) investigated the effect of pulp and matrix on the properties of TEMPO-CNF composites. In this study, EFB cellulose aerogel composite was prepared by incorporating graphene oxide (GO) into a matrix material as a second-phase filler in order to enhance the thermal stability and mechanical properties of the aerogel.

GO is a reinforcing material for natural polymers. The chemical functionalization of GO has been shown to enhance its dispersion in matrices (Yan et al. 2014). The hydrophilic oxygen-containing groups and hydrophobic basal plane of GO can react covalently or non-covalently with different compounds (Gan et al. 2017c). Biopolymers are one of the compounds that could promote the biocompatibility of composites without affecting overall performance by immobilizing covalently with the oxygen moieties of GO sheets (Gorgolis and Galiotis 2017). Huang and his coworkers, for example, have shown enhancement in the mechanical properties of cellulose paper via the incorporation of GO (Huang et al. 2016). There are few studies that demonstrate the effect of GO addition on the improvement of the thermal stability of cellulose aerogel composites, especially in the case of waste biomass. Due to the growing demand for environmentally friendly bio products, cellulose regeneration is an important possibility for shaping and processing of novel materials (Ahmed 2013; Pierre and Pajonk 2002). Cellulose can be recycled and it exhibits better properties in term of strength of material at each weight ratio which is suitable for producing composite materials (Eichhorn et al. 2001). Therefore, in our studies, the waste biomass of EFB cellulose was utilized as a matrix to produce GO-reinforced cellulose aerogel bionanocomposites. The preparation method is simple and environmentally friendly. In our study, the effect of GO concentrations on various properties of the GO/cellulose aerogel bionanocomposite will be highlighted.

Materials and methods

Materials

Graphite flakes, sodium hydroxide monohydrate ($NaOH \cdot H_2O$), epichlorohydrin (ECH), sulphuric acid (H_2SO_4) and urea (CH_4N_2O) were purchased from Sigma Aldrich. Sodium chlorite ($NaClO_2$) was obtained from Acros Organics. Hydrogen peroxide (H_2O_2) and hydrochloric acid (HCl) were purchased from Systerm. Sodium hydroxide (NaOH), potassium permanganate ($KMnO_4$), and ortho-phosphoric acid (H_3PO_4) were supplied by R & M Chemicals. The reagents used in this study as listed in Table 1 were of analytical grade and used as received. The oil palm EFB was soda pulped in the Forest Research Institute Malaysia (FRIM) in a digester with 25% NaOH concentration at 170 °C for 150 min. The EFB pulp was bleached in accordance with the methods as described in our previous paper (Gan et al. 2017a). The bleached EFB pulp was dried at 105 °C for 24 h and henceforth named as EP. Graphene oxide (GO) was synthesized using modified Hummers method as described in our previous report (Gan et al. 2015).

Preparation of GO/cellulose solution

A NaOH/urea aqueous solution was prepared with a weight ratio between NaOH, urea and water, as 7:12:81 wt% and stored in a freezer. As the solvent reached temperature of − 13 °C, 4 wt% of EP was dissolved in the urea alkaline aqueous solution via rapid dissolution method. The cellulose solution was then stirred vigorously for around 5 min to obtain a heterogeneous transparent cellulose solution. The cellulose solution underwent centrifugation for degassing and separating the dissolved cellulose and undissolved cellulose. After that, the obtained cellulose solution was mixed with a sonicated GO solution and was stirred in an ice bath for 30 min. A series of mixed GO/cellulose solutions were attained with GO concentrations of 0, 1, 2, 3 and 4 wt%.

Preparation of GO/cellulose aerogel bionanocomposite

The GO/cellulose solutions with various GO concentrations were combined dropwise with ECH for a cross linking process and stirred for an hour to create a

Table 1 List of chemicals used in this study

Chemical	Chemical formula	Purity (%)
Graphite flakes	C	99 ($\sim$ 325 mesh)
Sodium hydroxide monohydrate	$NaOH \cdot H_2O$	98
Epichlorohydrin	C_3H_5ClO	99
Sulphuric acid	H_2SO_4	95–98
Urea	$CO(NH_2)_2$	99
Sodium chlorite	$NaClO_2$	80
Hydrogen peroxide	H_2O_2	30
Hydrochloric acid	HCl	37
Sodium hydroxide	NaOH	97
Potassium permanganate	$KMnO_4$	97
Ortho-phosphoric acid	H_3PO_4	85

heterogeneous mixture. The GO/cellulose solution was then kept at low temperatures (3 °C) overnight for solidification process. The gel-like GO/cellulose hydrogel composites were soaked in a distilled water bath for cleaning and swelling purposes for 25 days. After that, the GO/cellulose hydrogels were freeze-dried (Scanvac CoolSafe 55-9 PRO 4lt freeze dryer, Model 55-9 from LaboGene) for 2 days to form GO/cellulose aerogels. The GO/cellulose aerogels that resulted from various GO concentrations (0, 1, 2, 3 and 4 wt%) were referred as CGA0, CGA1, CGA2, CGA3 and CGA4, respectively.

Characterizations

The GO/cellulose aerogel samples were cleaned and freeze-dried before being cut into powder form in 10 mg portions. The GO/cellulose aerogel samples were then characterized by TGA (Mettler Toledo TGA/SDTA851^e). TGA conditions included a heating rate of 10 °C/min over the temperature range from 25 to 600 °C in air. The cross-section of the freeze-dried aerogel sample was cut and sputter-coated with gold prior to FESEM examination. The morphology of GO/cellulose aerogel was viewed under FESEM (Zeiss/Supra 55VP). The density of the GO/cellulose aerogel was measured using an electronic densitometer (MD 300S-ALFA Mirage). The pore volume of the GO/cellulose aerogel was calculated using the formula: $V_p = \frac{M_{wet} - M_{dry}}{\rho \times M_{dry}}$ where ρ is the density of water (0.995 g/cm^3), and M_{wet} and M_{dry} are the weight of wet and dry GO/cellulose aerogel samples, respectively (Li et al. 2014). The porosity of GO/cellulose

aerogel was computed using the following equation: $porosity\ (\%) = \left(1 - \frac{\rho_b}{\rho_s}\right) \times 100\%$, where ρ_b is the bulk density of cellulose aerogel and ρ_s is the skeleton density ($\rho_s = 0.6$ g/cm^3) (Liao et al. 2016).

The degree of swelling (DS) of GO/cellulose hydrogel (before drying into aerogel) was determined from the equation: DS $(\%) = \frac{W_s - W_d}{W_d} \times 100$ where W_d is the original weight of GO/cellulose hydrogel before immersing into the distilled water and W_s is the weight of GO/cellulose hydrogel achieved equilibrium in the distilled water. After freeze-drying the GO/cellulose hydrogel, the GO/cellulose aerogel (a dried form of hydrogel) was immersed again into the distilled water until it reached the equilibrium point, in order to measure the equilibrium-swelling ratio (Q). The equilibrium-swelling ratio of the GO/cellulose aerogel was calculated from formula: Q $(\%) = \frac{W_h - W_o}{W_o} \times 100$ where, W_h is the weight of the swollen GO/cellulose aerogel and W_o is the weight of GO/cellulose aerogel (Li et al. 2014). Five replicates for each sample (3 cm × 1 cm × 3 cm) were performed to obtain an average value of degree of swelling and equilibrium-swelling ratio.

The phase and degree of crystallinity (CrI) for GO/cellulose aerogels were determined using X-ray diffraction (XRD) (Bruker D8 Advance Madison, WI, USA) with CuKα radiation ($\lambda = 0.15458$ nm). The GO/cellulose aerogel samples were scanned from 5° to 50° 2θ. FT-IR (Perkin Elmer Spectrum 400) was used to examine functional groups of the GO/cellulose aerogel samples between 4000 and 800 cm^{-1} with 32 numbers of scans and resolution of measurement was set to 4 cm^{-1}.

Results and discussion

Thermal analysis

The thermal properties of GO/cellulose aerogel bio-nanocomposites were evaluated via thermogravimetric analysis (TGA) and derivative thermogravimetric analysis (DTG). The TGA and DTG results for the CGA samples at different GO concentrations are demonstrated in Fig. 1a, b, respectively. The TGA curves of all GO/cellulose aerogel composites exhibited two steps degradation. The first step of
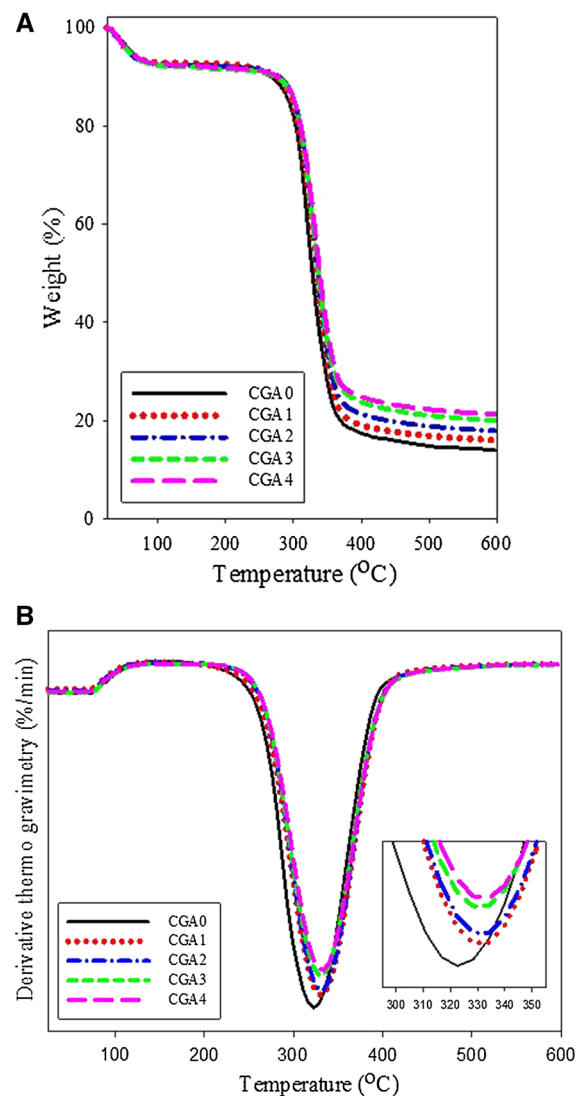
Fig. 1 a TGA of GO/cellulose aerogel bio-nanocomposites with different GO concentrations. **b** DTG of GO/cellulose aerogel bio-nanocomposites with different GO concentrations

degradation appeared at about 100 °C with the weight loss of 6.46%, which is probably caused by the evaporation of absorbed water. This trend has been previously observed by Yadav et al. (2013). The second degradation was observed when a remarkable weight loss happened in the temperature range of 229–425 °C. The details of the second step thermal degradation characteristics (T_o, T_{max} and T_f) of the GO/cellulose aerogel composite are listed in Table 2, in which the T_o value is defined as the initial decomposition temperature where the weight loss started, and the T_{max} is the temperature with maximum decomposition rate where the highest weight loss happened. T_f is the final decomposition temperature where the weight loss completed.

As the DTG curves of GO/cellulose aerogel composites shifted towards the right, the T_o, T_{max} and T_f values were higher than those of the pure cellulose aerogel (CGA0). This implies that the thermal stability of the aerogel composite was enhanced with the introduction of GO. This may be due to lots of epoxy, hydroxyl, and carbonyl groups on the surface of GO sheets which enhanced the formation of hydrogen bonds between GO and hydroxyl-rich cellulose. Hence, the good interaction between GO and cellulose could restrict the movement of the polymer segments at the interface of the cellulose and GO (Yao et al. 2014). Another possible reason for the improvement of thermal stability of cellulose could be the layered structure of the GO, which tends to offer only indirect pathways for the volatile degradation products, delaying the degradation of the whole composite (Chozhan et al. 2009). Similar results were also observed in previous findings such as Liu et al. (2017) who fabricated sodium alginate composite paper by reinforcing GO, and Zhang et al. (2012b) who produced chitosan film reinforced by GO.

As can be seen in Fig. 1a and Table 2, the minimum residue was produced at 500 °C of pure cellulose aerogel. Compared to the pure cellulose aerogel, the residues of the GO/cellulose aerogel bio-nanocomposites were higher. When the concentration of GO increased from 1 to 4 wt%, the amount of residual mass left over increased by about 14.7–50.3% accordingly. The residues corresponded to char yield in bio-nanocomposites, in which GO is well-known as the carbon based material and the combustion of GO generates char residues. Therefore, the char yield of the GO/cellulose aerogel composite was found to

Table 2 Thermal degradation characteristics of GO/cellulose aerogel bio-nanocomposite

Sample	Decomposition temperature (°C)			Residues after 500 °C (wt%)
	T_o	T_{max}	T_f	
CGA0	229	322	412	14.3
CGA1	237	331	417	16.4
CGA2	238	331	419	18.3
CGA3	238	331	420	20.2
CGA4	241	331	425	21.5

increase with the higher concentrations of GO. This increase of carbon yield proved advantageous as a carbon fibre precursor (Han et al. 2011a; Zhu and Wilkie 2000).

Comparison between experimental and modeled TGA curves

A rule of mixture (ROM) was employed to predict the modelling curves of weight loss for GO/cellulose aerogel bio-nanocomposites ($W_m(T)$) at the heating temperature (T) model with the following equation (Chen et al. 2016a): $W_m(T) = W_c(T) \times W_c + W_{GO}(T) \times W_{GO}$ where $W_m(T)$ is the weight loss of the GO/cellulose aerogels at temperature T and $W_c(T)$ and $W_{GO}(T)$ are the weight loss of pure cellulose and GO at temperature T, respectively. W_c and W_{GO} are the corresponding weight fractions of the two components in the GO/cellulose aerogel composites. The comparison between experimental curves and modeled curves for CGA1, CGA2, CGA3 and CGA4 GO/cellulose aerogels is demonstrated in Fig. 2.

The weight loss experimental curves of the GO/cellulose aerogel composites at different GO concentrations fit the ROM model curves reasonably well. As the temperature passes 200 °C, the experimental curves of all GO/cellulose aerogel composites shifted towards the right to the higher temperature as compared to the predicted curves. Furthermore, as the GO concentration increases, the difference in temperature between experimental curves and modeled curves increases at the same weight loss point. This indicates the delay of the decomposition of the GO/cellulose aerogel composites was achieved as discussed by Chen et al. (2016a). Compared to the modeled curves, the decomposition of the GO/cellulose aerogel composites in the study required higher temperature with the increase of GO concentrations. These results

confirmed that the introduction of GO has improved the thermal stability of GO/cellulose aerogel composites. All the char yields of the experimental were higher than that of the char yield of the modeled. It can also be seen that as the GO concentration increases, the difference in char yield of GO/cellulose aerogel composite between experimental curves and modeled curves increases.

Morphology analysis

Figure 3a portrays the SEM images of the cross-section of (a) CGA0, (b) CGA1, (c) CGA2, (d) CGA3 and (e) CGA4. All GO/cellulose aerogel bio-nanocomposites illustrated macroporous structure with average homogenous porosity similar to the results found in Tiwari et al. (2013) who prepared graphene oxide-based hydrogel to capture dye pollutants. The three dimensional networks with large interstitial spaces in the bulk of aerogel composites were produced via the connection among the long cellulose fibrils (Wang et al. 2012).

As proposed by Shi et al. (2015), during the cellulose dissolution in NaOH/urea solvent system, the negatively charge cellulose would react with Na^+ ions. This led to more water molecules entering the cellulose chains and swelling the cellulose molecules in aqueous solution. The water molecules were removed during the freeze-drying process of cellulose which created pores in the cellulose aerogels. In Fig. 3b, the schematic diagram of the macroporous formation of GO/cellulose aerogel composite is depicted. After adding the crosslinker (ECH) into the GO/cellulose solution as described in preparation of GO/cellulose aerogel bio-nanocomposites, the GO/cellulose solution became a kind of cross-linked gel (hydrogel) containing a large amount of solvent. This is due to the GO and ECH possibly reacting with the hydroxyl group of the anhydroglucose units in

Fig. 2 Comparison of thermogravimetric curves between the experimental and modeled curves for GO/cellulose aerogel bio-nanocomposites with different GO concentrations
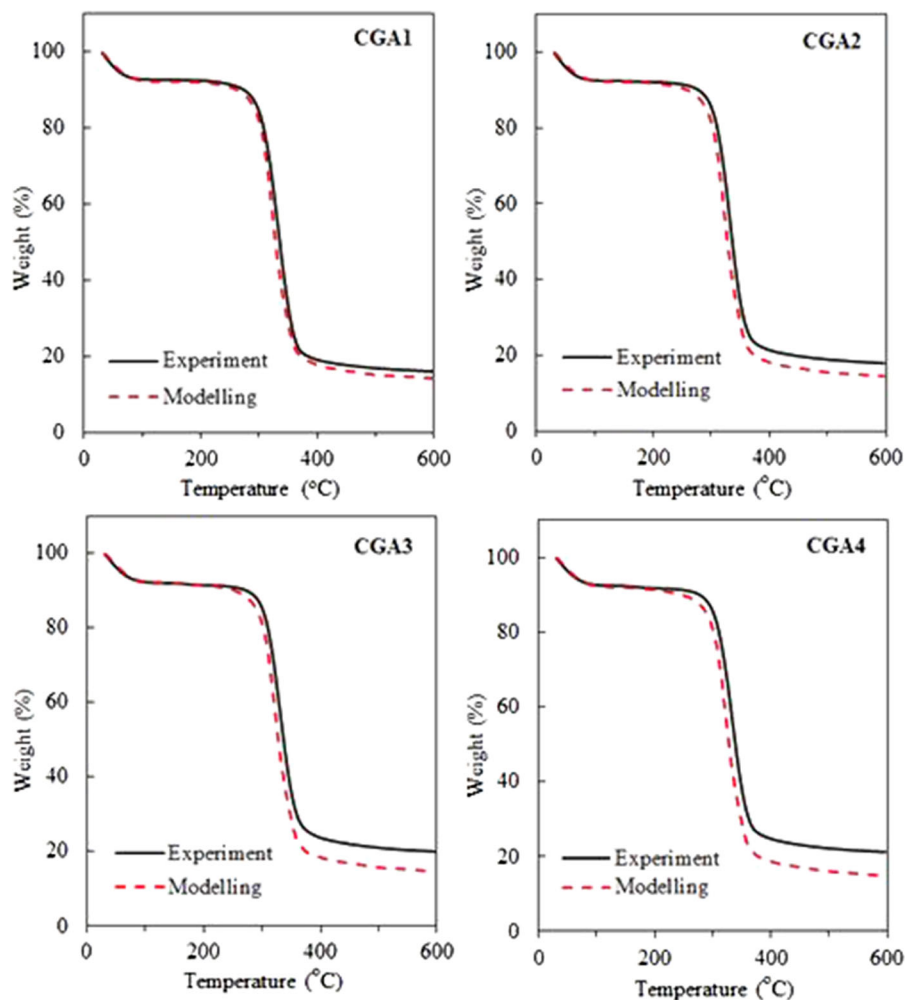
cellulose (Gan et al. 2017b). The chemically cross-linked gel (GO/cellulose hydrogel) was then immersed into the distilled water (non-solvent) and the H_2O diffused into the cross-linked gel for the solvent-exchange process. The pH of the GO/cellulose hydrogel will eventually achieve equilibrium and becomes neutral. The exchange of solvent and non-solvent played an important role in the reformation of intra- and inter hydrogen bonds that have previously been broken during the dissolution process, in terms of mechanistic aspects (Lindman et al. 2017).

The type of solvent and non-solvent interactions could significantly affect the morphological and mechanical properties of the regenerated cellulose, as proposed by Lindman et al. (2017). Hence the non-solvent water plays a relevant role in this study. During the freeze-drying process, the trapped water in

the swollen GO/cellulose hydrogel turned into ice crystals with phase separation at 0 °C. When the temperature was lower than − 18 °C, sublimation started to occur and turn the ice crystals into voids in the GO/cellulose aerogels. The reason GO/cellulose aerogel composite became a macroporous rigid structure is probably due to the precipitation of cellulose chains in the solvent as illustrated in Fig. 3b.

Density, pore volume and porosity

The density, pore volume, and porosity of GO/cellulose aerogel bionanocomposites are shown in Fig. 4. The porosity and pore volume of the GO/cellulose aerogel composites were negatively correlated with the increase of GO concentrations. However, the density of the GO/cellulose aerogel composites

Fig. 3 a Morphology of
(a) CGA0, (b) CGA1,
(c) CGA2, (d) CGA3 and
(e) CGA4 GO/cellulose
aerogel bio-
nanocomposites.
b Schematic diagram of the
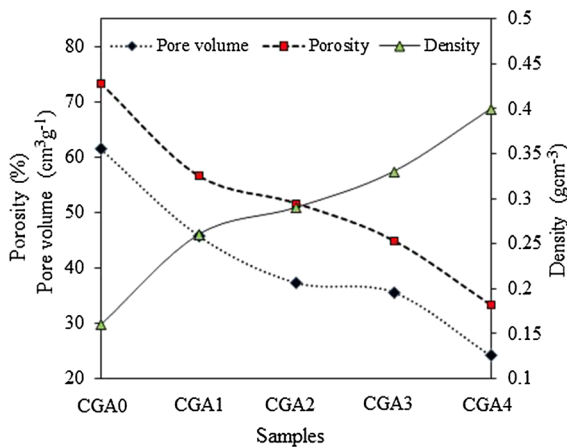macroporous formation of
GO/cellulose aerogel bio-
nanocomposites
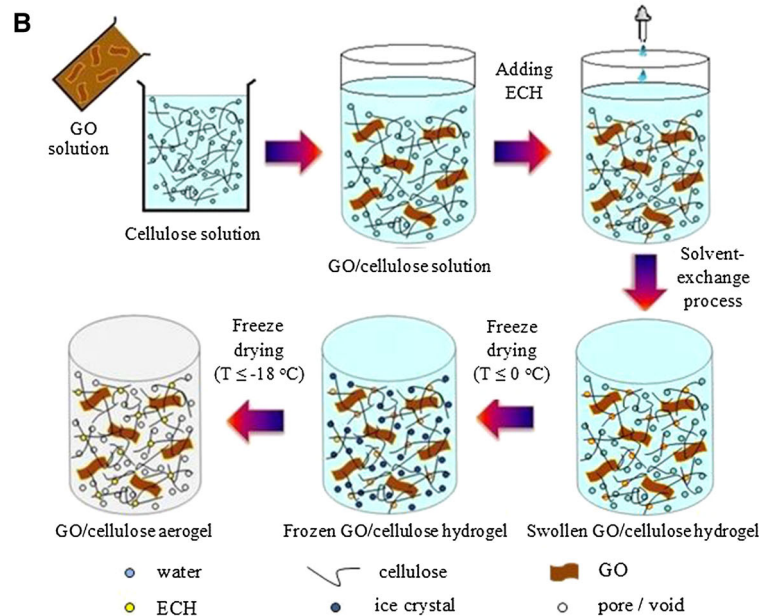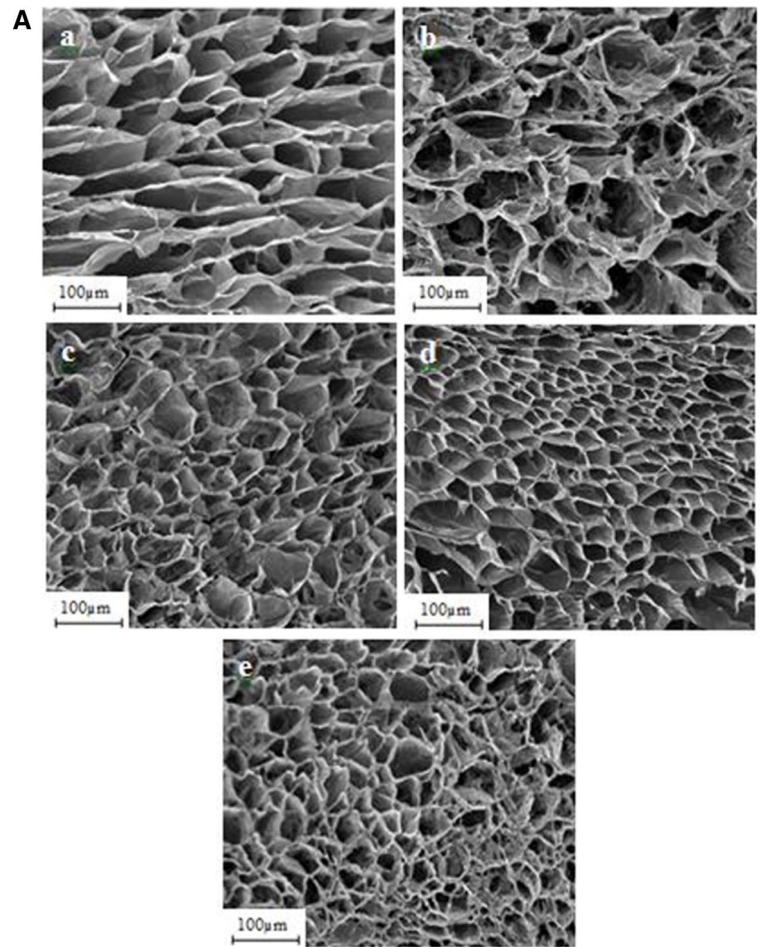
Fig. 4 Physical properties of GO/cellulose aerogel bio-nanocomposites

Fig. 5 The degree of swelling and equilibrium-swelling ratio of GO/cellulose aerogel bio-nanocomposites with different GO concentrations

increased gradually with the increase of GO. As evidenced in Fig. 3a, the pore volume of the GO/cellulose aerogel composites decreased with the rise of GO concentration. The pore volume of CGA0 was about 60% lower than CGA4. CGA4 possessed the lowest porosity (about 33%).

This indicates that the addition of the GO sheets may block some of the pores in the aerogel composite, resulting in a reduction in the porosity of the GO/cellulose aerogel composites. As a result, less water molecules could penetrate into the GO/cellulose aerogel composite and be trapped in the pores. This finding was also in agreement with the decrease in degree of swelling and equilibrium-swelling ratio of GO/cellulose aerogel composite (discussed further on). The decrease in the porosity directly correlated to the increase of the density of the aerogel composite. Hence, the density of the GO/cellulose aerogel composites slightly decreased from 0.4 to 0.16 gcm^{-3} with the increase of the GO concentrations, which was similar to the density of pure cellulose aerogel as studied by Shi et al. (2015).

Degree of swelling and equilibrium-swelling ratio

The degree of swelling and equilibrium-swelling ratio properties are presented in Fig. 5. A chemically cross-linked network is usually needed to form a stable hydrogel and aerogel structure. Similar to previous studies (Chen et al. 2016b; Gan et al. 2017a), the common cross-linker ECH was employed in the study to bind the cellulose molecules covalently in a three
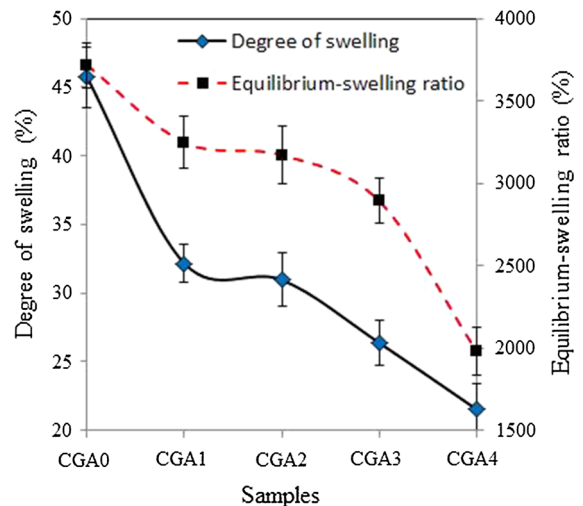
dimensional hydrophilic network as presented in Fig. 3. The chemical reaction of cellulose and epichlorohydrin in the hydrogel has been discussed in our earlier paper Gan et al. (2017b).

Stable three dimensional hydrophilic networks allowed water to penetrate into the hydrogel and the aerogel composite structure. This could break up the binding force in the non-crystalline area of the cellulose and disturb the crystalline area of the cellulose (which will be discussed later). Interestingly, with the incorporation of GO, both porosity and pore volume of the aerogel composites decreased as presented in Fig. 4. This result is in agreement with the reduction of degree of swelling in hydrogel composites as the GO concentrations increased. It was also found that the equilibrium-swelling ratio of the GO/cellulose aerogel composites exhibited a similar trend, which was a downward trend with the increasing GO concentrations. This is presumed to be due to the fact that the introduction of GO sheets has increased the density of the structure and blocks the pores in the aerogel. Thus, the increase in the concentration of GO limits the total amount of water diffuses and traps in the GO/cellulose aerogel composite, leadingto a lower equilibrium-swelling ratio.

XRD pattern

The XRD patterns of EP, GO, CGA0 and CGA4 are illustrated in Fig. 6. The EP showed typical allomorph of cellulose I with distinct peaks at $2\theta = 14.8°$, $16.3°$ and $22.7°$ (Gan et al. 2015; Han et al. 2011b). They typical GO peak at $9.9°$ (001) indicates a spacing of about 8.9 Å, providing for the oxygen on the graphene sheets and the water molecules trapped among the GO sheets (Feng et al. 2012). Upon dissolution and regeneration of cellulose, regenerated cellulose aerogel (CGA0) and GO/cellulose aerogels bio-nanocomposites (CGA4) exhibited cellulose II crystalline structure with peaks located at $2\theta = 12°$ and $20.2°$. The intensity of the peaks was weakened, indicating that the decreased cellulose crystallinity is due to the destruction of crystalline structure in cellulose via breakage of hydrogen bonds. During the dissolution and regeneration process, the rapid proton exchange of hydroxyl groups in cellulose with the solvent molecules lead to an unrecovered hydrogen bond network structure (Zhang et al. 2017a). This process, as well as the crosslinking reaction between the cellulose molecules and ECH, haas promoted the formation of amorphous area in cellulose aerogel structure (Ding

et al. 2012). Hence, it is shown that cellulose I of EP has been successfully transformed into cellulose II (regenerated cellulose aerogel) upon dissolution and regeneration process as shown in Padzil et al. (2015).

However, the (001) peak of GO did not exist in the CGA4 sample which might be due to the good dispersion and exfoliation of GO in the cellulose solution upon mixing (Feng et al. 2012; Gan et al. 2015; Han et al. 2011b). Chen et al. (2016b) proposed that bond interaction among GO sheets and cellulose molecules was the main reason thatthe characteristic peak of GO did not exist in the XRD pattern of GO/cellulose aerogel composites. This can be further explained by the occurrence of the periodic interlayer spacing between the GO sheets after dissolution process. In addition, the diffraction peaks of CGA0 without GO concentration was similar to that of the CGA4. This suggests that GO/cellulose aerogel composite has also formed into cellulose II allomorph (Liu et al. 2016). Moreover, this is indicating that GO sheets were well exfoliated in the cellulose matrix and the introduction of GO did not affect on the amorphous structure of cellulose as agreed by Yadav et al. (2013). The GO/cellulose hydrogel composite was black in colour when compared to pure cellulose hydrogel that

Fig. 6 XRD pattern of EP, GO, CGA0 and CGA4
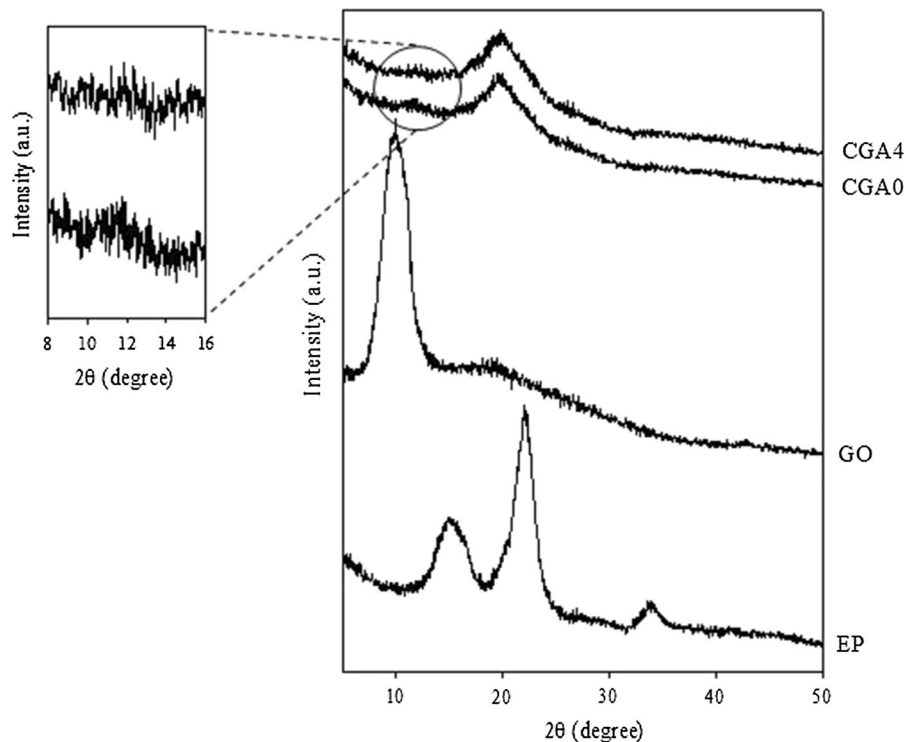
was transparent after solidification process. This implies the reduction of GO has taken place to some extent in the cellulose solution containing urea and alkaline (Han et al. 2011b).

This diffraction study is generally conducted on cellulose to determine degree of crystallinity and polymorph identity, (French 2014). The degrees of crystallinity of EP, CGA0 and CGA4 were 66.5 ± 1.4, 47.2 ± 0.8 and 43.9 ± 1.1, respectively. The native cellulose, EP, had the highest crystallinity. This is possibly due to native cellulose containing of high amount of strong inter- and intra- hydrogen bonding with the cellulose chains occuring in a well-arranged cellulose structure. After cellulose is completely dissolved into individual molecules with random orientations and conformations, the regeneration process can only result in relatively small crystalline regions. The CGA4 showed a lower degree of crystallinity than CGA0 due to the introduction of the amorphous state of GO in GO/cellulose aerogel composites which disturbed the degree of crystallinity (Feng et al. 2012; Ouyang et al. 2013). Liu et al. (2016) proposed that chemically cross-linked molecules of cellulose and GO sheets may result in the reduction of degree of crystallinity.

FTIR spectra

Figure 7 depicts the FTIR spectra of GO, EP, CGA0, CGA1, CGA2, CGA3 and CGA4. The transmittance peaks of the EP and regenerated aerogel composites were almost the same. Both raw EP and aerogel composites exhibited significant characteristic transmittance peaks of cellulose macromolecular which indicated that cellulose did not derivate in the cellulose dissolution process. Hence, the EP was dissolved directly in the dissolution course as discussed by Shi et al. (2015). The broad peaks located at GO spectrum confirmed the oxidation of graphite to GO as discussed in previous literature. In FTIR spectrum of GO, the strong peaks of 3354 and $3257 \mathrm{~cm}^{-1}$ corresponded to –OH functional group and the transmittance band peak at $1630 \mathrm{~cm}^{-1}$ was assigned to the double carbon bonding (C=C) of the aromatic rings of the GO carbon skeleton structure. The FTIR spectrum of EP exhibited the diffraction curve of typical cellulose structure. The transmittance band of approximately $3360 \mathrm{~cm}^{-1}$ was referred to the –OH stretching vibration. Moreover, the occurrence of
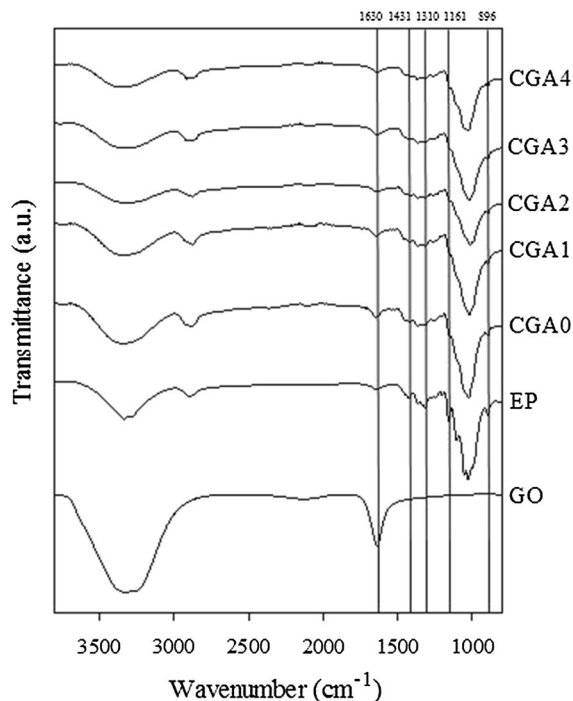

Fig. 7 FTIR spectra of GO, EP, and GO/cellulose aerogel bionanocomposites with different GO concentrations

the peak at $2920 \mathrm{~cm}^{-1}$ corresponded to the C–H stretching vibration. The alcoholic group of C–OH for EP was observed by the appearance of the peaks at 1010 and $1160 \mathrm{~cm}^{-1}$. In which other peaks appeared at 1370 and $1310 \mathrm{~cm}^{-1}$ represented the existence of CH_2 bending vibration.

FTIR spectra of the GO/cellulose aerogels bionanocomposites demonstrated the absorption characteristic of cellulose II. There is an increase in intensity of CGA0 sample located at $896 \mathrm{~cm}^{-1}$ which represents the non-crystalline area of cellulose as compared to the EP native cellulose. Moreover, this band has shifted to a lower wavenumber in comparison with that of the EP. This shows that the cellulose I has been transformed into cellulose II allomorph during the formation of aerogel from EP as with Liu and Zhang (2009). As compared to the EP native cellulose, the bands at 1431 and $1310 \mathrm{~cm}^{-1}$ in all GO/cellulose aerogels, which corresponded with the symmetric bending and wagging of –CH_2 have moved to lower wavenumber. This is probably due to the disturbance of intermolecular hydrogen bonding involved O_6 exocyclic hydroxyl groups during the dissolution process. This has also confirmed the transformation

from cellulose I to cellulose during the dissolution and regeneration process in the formation of aerogel with or without GO (Sang et al. 2005). The CGA0 sample presented the similar characteristic absorption as the curve of pure cellulose (EP). The GO/cellulose aerogel composites (CGA1, CGA2, CGA3 and CGA4) exhibited combined characteristics of the EP and GO which included the broad transmittance band situated at 3360 cm^{-1} that corresponded to the –OH groups in the cellulose and GO. The occurrence of the broaden transmittance peaks at 1620, 1410, 1228 and 1060 cm^{-1} suggested the successful blending of the cellulose with the GO.

Conclusions

A facile method has been proposed to prepare GO/cellulose aerogel composites that feature thermal stability from waste biomass. The XRD and FTIR characterization confirm the regeneration process from EFB cellulose (cellulose I) to GO/cellulose aerogel composites (cellulose II). By employing the rule of mixture (ROM), the experimental and modelling results of the GO/cellulose aerogel composites could be compared in terms of thermal properties. The experimental results of GO/cellulose aerogel composites were proven to exhibit greater thermal stability than the modelling results. This is due to the decomposition or degradation of the experimental result of GO/cellulose aerogel composites required higher temperatures as compared to the predicted modelling results. The GO/cellulose aerogel composites showed a macroporous structure with equilibrium-swelling ratio in the range of 2000 and 3700%. The preparation of GO/cellulose aerogel bio-nanocomposite from waste biomass with environmentally friendly and thermostability features may have promising applications especially in the field of thermal insulating. From the industrial perspective, although several studies are attempting to produce aerogels with low density and high flexibility, the production cost and mechanical properties of the aerogel should be taken into the consideration. Hence, the preparation of aerogel bio-nanocomposite from waste biomass could be an alternative to reduce the production cost.

References

Ahmadzadeh A, Zakaria S (2007) Kinetics of oil palm empty fruit bunch phenolysis in the presence of sulfuric acid as a catalyst. J Appl Polym Sci 106:3529–3533

Ahmed EM (2013) Hydrogel: preparation, characterization, and applications. J Adv Res 6:105–121

Azahari NA, Zakaria S, Kaco H, Gan S, Chia CH, Jaafar SNS, Sajab MS (2017) Membran Selulosa Kenaf Terjana Semula daripada Larutan Akues NaOH/Urea yang Digumpal Menggunakan Asid Sulfurik. Sains Malays 46:795–801

Chen RS, Ahmad S, Gan S, Salleh MN, Ab Ghani MH, Tarawneh MAA (2016a) Effect of polymer blend matrix compatibility and fibre reinforcement content on thermal stability and flammability of ecocomposites made from waste materials. Thermochim Acta 640:52–61. https://doi.org/10.1016/j.tca.2016.08.005

Chen X, Zhou S, Zhang L, You T, Xu F (2016b) Adsorption of heavy metals by graphene oxide/cellulose hydrogel prepared from NaOH/urea aqueous solution. Materials 9:1–15

Chozhan CK, Alagar M, Gnanasundaram P (2009) Synthesis and characterization of 1,1-bis(3-methyl-4-hydroxy phenyl)cyclohexane polybenzoxazine-organoclay hybrid nanocomposites. Acta Mater 57:782–795

Ding Z-D, Chi Z, Gu W-X, Gu S-M, Liu J-H, Wang H-J (2012) Theoretical and experimental investigation on dissolution and regeneration of cellulose in ionic liquid. Carbohydr Polym 89:7–16. https://doi.org/10.1016/j.carbpol.2012.01.080

Eichhorn SJ et al (2001) Review: current international research into cellulosic fibres and composites. J Mater Sci 36:2107–2131. https://doi.org/10.1023/A:1017512029696

Feng Y, Zhang X, Shen Y, Yoshino K, Feng W (2012) A mechanically strong, flexible and conductive film based on bacterial cellulose/graphene nanocomposite. Carbohydr Polym 87:644–649. https://doi.org/10.1016/j.carbpol.2011.08.039

French A (2014) Idealized powder diffraction patterns for cellulose polymorphs. Cellulose 21:885–896. https://doi.org/10.1007/s10570-013-0030-4

Gan S, Zakaria S, Chia CH, Chen RS, Jeyalaldeen N (2015) Physico-mechanical properties of a microwave-irradiated kenaf carbamate/graphene oxide membrane. Cellulose 22:3851–3863

Gan S, Zakaria S, Chen RS, Chia CH, Padzil FNM, Moosavi S (2017a) Autohydrolysis processing as an alternative to enhance cellulose solubility and preparation of its regenerated bio-based materials. Mater Chem Phys 192:181–189. https://doi.org/10.1016/j.matchemphys.2017.01.012

Gan S, Zakaria S, Chia CH, Chen RS, Ellis AV, Kaco H (2017b) Highly porous regenerated cellulose hydrogel and aerogel prepared from hydrothermal synthesized cellulose carbamate. PLoS ONE 12:e0173743

Gan S, Zakaria S, Jaafar SNS (2017c) Enhanced mechanical properties of hydrothermal carbamated cellulose nanocomposite film reinforced with graphene oxide. Carbohydr Polym 172:248–293

Gorgolis G, Galiotis C (2017) Graphene aerogels: a review. 2D Mater 4:032001–032021

Han D, Yan L, Chen W, Li W (2011a) Preparation of chitosan/graphene oxide composite film with enhanced mechanical strength in the wet state. Carbohydr Polym 83:653–658. https://doi.org/10.1016/j.carbpol.2010.08.038

Han D, Yan L, Chen W, Li W, Bangal PR (2011b) Cellulose/graphite oxide composite films with improved mechanical properties over a wide range of temperature. Carbohydr Polym 83:966–972. https://doi.org/10.1016/j.carbpol.2010.09.006

Huang Q, Xu M, Sun R, Wang X (2016) Large scale preparation of graphene oxide/cellulose paper with improved mechanical performance and gas barrier properties by conventional papermaking method. Ind Crops Prod 85:198–203. https://doi.org/10.1016/j.indcrop.2016.03.006

Li W, Wu Y, Liang W, Li B, Liu S (2014) Reduction of the water wettability of cellulose film through controlled heterogeneous modification. ACS Appl Mater Interfaces 6:5726–5734

Liao Q, Su X, Zhu W, Hua W, Qian Z, Liu L, Yao J (2016) Flexible and durable cellulose aerogels for highly effective oil/water separation RSC. Advances 6:63773–63781

Lindman B, Medronho B, Alves L, Costa C, Edlund H, Norgren M (2017) The relevance of cellulose structural features and interactions on dissolution, regeneration, gelation and plasticization phenomena. Phys Chem Chem Phys 19:23704–23718

Liu S, Zhang L (2009) Effects of polymer concentration and coagulation temperature on the properties of regenerated cellulose films prepared from LiOH/urea solution. Cellulose 16:189–198

Liu X, Zhang T, Pang K, Duan Y, Zhang J (2016) Graphene oxide/cellulose composite films with enhanced UV-shielding and mechanical properties prepared in NaOH/urea aqueous solution. RSC Adv 6:73358–73364. https://doi.org/10.1039/C6RA16535D

Liu S, Ling J, Li K, Yao F, Oderinde O, Zhang Z, Fu G (2017) Bio-inspired and lanthanide-induced hierarchical sodium alginate/graphene oxide composite paper with enhanced physicochemical properties. Compos Sci Technol 145:62–70. https://doi.org/10.1016/j.compscitech.2017.01.009

Mohd Nor NS et al (2015) Influence of gamma irradiation exposure on the performance of supercapacitor electrodes made from oil palm empty fruit bunches. Energy 79:183–194. https://doi.org/10.1016/j.energy.2014.11.002

Ng P, Chia CH, Zakaria S, Gan S, Kaco H, Padzil FNM, Chook SW (2015) Preparation of cellulose hydrogel from oil palm empty fruit bunch fibers cellulose. Polym Res J 9:449

Ouyang W, Sun J, Memon J, Wang C, Geng J, Huang Y (2013) Scalable preparation of three-dimensional porous structures of reduced graphene oxide/cellulose composites and their application in supercapacitors. Carbon 62:501–509. https://doi.org/10.1016/j.carbon.2013.06.049

Padzil FNM, Zakaria S, Chia CH, Jaafar SNS, Kaco H, Gan S, Ng P (2015) Effect of acid hydrolysis on regenerated kenaf core membrane produced using aqueous alkaline–urea systems. Carbohydr Polym 124:164–171. https://doi.org/10.1016/j.carbpol.2015.02.013

Pierre AC, Pajonk GM (2002) Chemistry of aerogels and their applications. Chem Rev 102:4243–4266. https://doi.org/10.1021/cr0101306

Poyraz B, Tozluoğlu A, Candan Z, Demir A (2017a) Matrix impact on the mechanical, thermal and electrical properties of microfluidized nanofibrillated cellulose composites. J Polym Eng. https://doi.org/10.1515/polyeng-2017-0022

Poyraz B, Tozluoğlu A, Candan Z, Demir A, Yavuz M (2017b) Influence of PVA and silica on chemical, thermo-mechanical and electrical properties of celluclast-treated nanofibrillated cellulose composites. Int J Biol Macromol 104:384–392

Sang YO et al (2005) Crystalline structure analysis of cellulose treated with sodium hydroxide and carbon dioxide by means of X-ray diffraction and FTIR spectroscopy. Carbohydr Res 340:2376–2391. https://doi.org/10.1016/j.carres.2005.08.007

Sarwar MS, Niazi MBK, Jahan Z, Ahmad T, Hussain A (2018) Preparation and characterization of PVA/nanocellulose/Ag nanocomposite films for antimicrobial food packaging. Carbohydr Polym 184:453–464. https://doi.org/10.1016/j.carbpol.2017.12.068

Shi J, Lu L, Guo W, Liu M, Cao Y (2015) On preparation, structure and performance of high porosity bulk cellulose aerogel. Plast Rubber Compos 44:26–32

Tiwari JN, Mahesh K, Le NH, Kemp KC, Timilsina R, Tiwari RN, Kim KS (2013) Reduced graphene oxide-based hydrogels for the efficient capture of dye pollutants from aqueous solutions. Carbon 56:173–182

Tozluoglu A, Poyraz B, Candan Z (2018) Examining the efficiency of mechanic/enzymatic pretreatments in micro/nanofibrillated cellulose production. Maderas Cienc Tecnol 20:67–84

Tozluoğlu A, Poyraz B, Candan Z, Yavuz M, Arslan R (2017) Biofilms from micro/nanocellulose of \hbox NaBH_{4}-modified kraft pulp. Bull Mater Sci 40:699–710

Tozluoğlu A et al (2018) TEMPO-treated CNF composites: pulp and matrix effect. Fibers Polym 19:195. https://doi.org/10.1007/s12221-018-7673-y

Wang Z, Liu S, Matsumoto Y, Kuga S (2012) Cellulose gel and aerogel from LiCl/DMSO solution. Cellulose 19:393–399

Yadav M, Rhee K, Jung I, Park S (2013) Eco-friendly synthesis, characterization and properties of a sodium carboxymethyl cellulose/graphene oxide nanocomposite film. Cellulose 20:687–698

Yan H, Tao X, Yang Z, Li K, Yang H, Li A, Cheng R (2014) Effects of the oxidation degree of graphene oxide on the adsorption of methylene blue. J Hazard Mater 268:191–198

Yao L, Lu Y, Wang Y, Hu L (2014) Effect of graphene oxide on the solution rheology and the film structure and properties of cellulose carbamate. Carbon 69:552–562. https://doi.org/10.1016/j.carbon.2013.12.066

Zhang J, Cao Y, Feng J, Wu P (2012a) Graphene-oxide-sheet-induced gelation of cellulose and promoted mechanical properties of composite aerogels. J Phys Chem C 116:8063–8068

Zhang X, Liu X, Zheng W, Zhu J (2012b) Regenerated cellulose/graphene nanocomposite films prepared in DMAC/LiCl solution. Carbohydr Polym 88:26–30. https://doi.org/10.1016/j.carbpol.2011.11.054

Zhang H et al (2017a) Facile cellulose dissolution and characterization in the newly synthesized 1,3-diallyl-2-ethylimidazolium acetate ionic liquid. Polymers 9:526

Zhang X, Jing S, Chen Z, Zhong L, Liu Q, Peng X, Sun R (2017b) Fabricating 3D hierarchical porous TiO_2 and SiO_2 with high specific surface area by using nanofibril-interconnected cellulose aerogel as a new biotemplate. Ind Crops Prod 109:790–802. https://doi.org/10.1016/j.indcrop.2017.09.047

Zhu J, Wilkie CA (2000) Thermal and fire studies on polystyrene–clay nanocomposites. Polym Int 49:1158–1163